Journal of Catalysis **187,** 464–473 (1999)
Article ID jcat.1999.2602, available online at http://www.idealibrary.com on IDEAL®

Hydrogen Activation and Reactivity of Ruthenium Sulfide Catalysts: Influence of the Dispersion

Claire Dumonteil,* Michel Lacroix,* Christophe Geantet,* Hervé Jobic,* and Michèle Breysse†,[1]

**Institut de Recherches sur la Catalyse, 2, Avenue Albert Einstein, 69626 Villeurbanne Cédex; and †Laboratoire de Réactivité de Surface, Université P. et M. Curie, 4, place jussieu, Casier 178, 75252, Paris Cedex 05, France*

Received April 19, 1999; revised June 9, 1999; accepted June 9, 1999

In order to examine the influence of the size of particles on the catalytic properties of sulfide catalysts, a series of ruthenium sulfide based catalysts, dispersed in a KY zeolite, supported on silica or unsupported, were prepared and characterized. Such a methodology allowed us to vary the particle size in a large domain. The particle sizes were determined by HREM for RuS_2/silica (3.6 nm) and the unsupported sample (5 nm) and by SAXS for the zeolite catalyst (1.2 nm). From these measurements, the fractions of ruthenium and sulfur present at the surface of the catalysts were deduced. The TPR patterns of the three catalysts exhibit three peaks whose relative proportions were also related to the amount of surface sulfur. An excellent agreement was observed between both kinds of determination. Then, the influence of a progressive reduction of the surface on the adsorbing and catalytic properties of the three samples was studied in the whole S/Ru range. Striking similarities were observed for the three catalysts concerning the nature of the hydrogen species and the variation of the hydrogenation activity with S/Ru. Indeed, inelastic neutron scattering revealed the presence of hydride species, as was already observed for unsupported RuS_2. The determination by TPD of the amount of hydrogen adsorbed and the measurements of catalytic activities allowed the determination of the turnover frequency for the catalysts of the present series. It appeared that these values are almost similar, which shows that the same active phase can be obtained as unsupported catalyst or highly dispersed in a zeolite. The interest of using this KY zeolite is to stabilize nanoparticles of sulfide phase inside its framework and consequently to obtain a high number of active sites.

Key Words: **hydrotreatment catalyst; transition metal sulfide; hydrogen activation; ruthenium sulfide; turnover number; dispersion; inelastic neutron scattering.**

INTRODUCTION

The comparison of the properties of various kinds of catalysts for a given reaction is generally achieved using the concept of turnover frequency or turnover number. This has allowed Boudart's subdivision of reactions into "structure-sensitive" and "structure insensitive" categories. A catalytic reaction is said to be structure-sensitive if its rate changes markedly as the particle size of the catalyst is changed; conversely, the rate of a structure-insensitive reaction is not significantly modified by such modifications. However, in heterogeneous catalysis, it is sometimes difficult to determine the number of active sites. For a finely dispersed supported-metal catalyst, physicochemical techniques such as high resolution electron microscopy and probe molecule adsorption allow us at least to count the number of surface atoms. For sulfide catalysts, which represent a very important class of catalysts, the determination of the number of active sites is even more difficult for several reasons, (i) the active sites are created *in situ* in reaction conditions, (ii) the structure of the most utilized sulfide phase, i.e., molybdenum sulfide, is anisotropic, and (iii) the relation between the probe molecule adsorption and the catalytic properties, even for a simple reaction, is not straightforward. To overcome some of these difficulties we chose ruthenium sulfide as a model catalyst because of its cubic structure and its high activity for most of the hydrotreating reactions (hydrogenation and hydrodesulfurization) (1, 2). A comprehensive study of the properties of an unsupported ruthenium sulfide catalyst, whose number of sulfur vacancies is monitored in a wide range by the means of reducing treatment, has allowed us to relate the catalytic properties for hydrogenation reactions to the concentration of hydrogen adsorbed as hydridic species (3).

In order to determine the influence of the dispersion, the same phase might be prepared in the supported state. However, it was shown for oxide supports that whatever the preparation and activation conditions, the particle sizes of ruthenium sulfide do not vary to a large extent (4). The use of a zeolite support might allow us to stabilize very small particles as shown in a previous study (5). Consequently, to address the influence of the dispersion on the activity, the comparison of the properties of ruthenium sulfide unsupported, supported on silica, or dispersed in a KY zeolite was undertaken. These supports were chosen in order to avoid any superimposed influence of the acidity. Moreover, the

[1] All correspondence should be sent to M. Breysse. Fax: (33) 01 44 27 60 33. E-mail: breysse@ccr.jussieu.fr.

0021-9517/99 $30.00

present work is part of a comprehensive study related to the properties of ruthenium sulfide dispersed in HY and KY zeolites (5, 6).

As for the previous studies, various techniques were used for the determination of the number of ruthenium and sulfur exposed atoms, HREM, SAXS, and temperature-programmed reduction. Hydrogen adsorption was studied as a function of the concentration of sulfur vacancies created by reducing treatment (7). As previously reported for the unsupported ruthenium sulfide, inelastic neutron scattering was used to determine the nature of hydrogen species, and the catalytic properties were evaluated for the H_2–D_2 exchange reaction (3).

EXPERIMENTAL

Catalyst Preparation

Ruthenium sulfide was prepared by precipitation at room temperature from an aqueous solution of $RuCl_3$ by pure H_2S and by further sulfidation in an H_2S flow at 673 K for 2 h. The catalyst was cooled to room temperature under the same atmosphere and flushed with an inert gas. X-ray diffraction was similar to that of RuS_2 reported in the JCPDS index, and elemental analysis indicated a stoichiometry S/Ru = 2.27. Its surface area determined by N_2 physisorption was 70 $m^2 g^{-1}$.

Silica-supported ruthenium sulfide was prepared using the pore filling method. The support is a Davidson 432 silica of 300 $m^2 g^{-1}$ BET area, having a pore volume of 0.5 $cm^3 g^{-1}$, which was dried overnight at 383 K prior to the impregnation. Aqueous solution of $RuCl_3$ was used as ruthenium salt precursor. After impregnation at room temperature for 3 h, the solid was dried at 383 K under vacuum before its transformation into a sulfided phase. This sulfidation step was performed by heating the precursor at 673 K in a 15% H_2S–85% N_2 atmosphere in order to avoid the intermediate formation of a metallic phase which is known to be difficult to sulfide (8). After this activation procedure, the solid was cooled to room temperature under the sulfiding atmosphere and flushed with an inert gas. The ruthenium content determined by chemical analysis was 7.5% and the catalyst composition corresponded to $RuS_{2.7}$ with a residual chlorine content lower than 0.01%.

The KY zeolite was prepared from NaY, supplied by Union Carbide (Type LZ-Y52), by three successive ion exchanges in an aqueous solution of KNO_3 (1 M) at 333 K for 24 h. Between each exchange the solid was washed with water at room temperature in order to eliminate $NaNO_3$. The ruthenium catalyst was prepared by ion exchange by stirring the KY zeolite in an aqueous solution of $[Ru(NH_3)_6]Cl_3$ (supplied from Johnson-Matthey), at room temperature for 48 h. The sulfidation of the catalyst was achieved in similar conditions as those utilized for the silica-supported sample. The chemical composition and NMR Si/Al ratio of the support and those of the ruthenium catalyst after sulfidation are given in Table 1. The Si/Al ratio determined by chemical analysis for the zeolite exchanged with ruthenium and further sulfided is very close to the values obtained for the starting zeolite, which indicates that there is no change in the overall composition of the zeolite. The ^{29}Si NMR gave results comparable to those of chemical analysis for the starting material, but after introduction of the ruthenium and sulfidation the Si/Al ratio increased from 2.4 to 5.8. This dealumination process was already observed after H_2S treatment in our previous study (6) and was compared to the dealumination process of zeolites by treatment with water vapor.

TABLE 1

Elemental Chemical Analysis and ^{29}Si NMR of KY Zeolite and RuS_2/KY

Catalyst:	Concentration (wt%) Si	Al	Na	K	Ru	S	S/Ru	Si/Al (from NMR)
KY	27.4	10.4	0.2	14.7	—	—		2.4
RuS_2/KY	26.4	10	n.d.	5.1	8.3	6.5	2.5	5.8

The catalysts will be referred to as RuS_2, RuS_2/SiO_2, and RuS_2/KY.

Electron Microscopy

High resolution electron microscopy (HREM) examinations were performed with a JEOL 100 CX instrument fitted with a UHP polar piece (resolving power 0.2 nm). The samples were ultrasonically dispersed in deoxygenated heptane at room temperature and the suspensions were collected on a carbon-coated copper grid. Particle size distribution was determined by counting about 400–600 particles. The average particle size was calculated according to the first moment of the distribution:

$$L = \frac{\sum_{i=1}^{n} n_i l_i}{\sum_{i=1}^{n} n_i}.$$

Small Angle X-Ray Scattering (SAXS)

The measurements were performed on a home-made apparatus, fitted with a Guinier-type collimation system (9). The particle size distribution was calculated from a Patterson function, obtained through Fourier transformation of the data. The volume distribution function, F_v (F index V), which is derived corresponds to the fractions of sample volume with constant size intervals.

TPR and Solid Reduction

Temperature programmed reduction experiments were carried out in a dynamic microreactor which allowed the measurement of the amount of H_2S removed under

hydrogen by the use of a specific UV photodetector ($h\nu$ photoionization detector equipped with a 10.21 eV UV light source). The detector was calibrated before each experiment with a H_2S/H_2 mixture of known composition. The sample was flushed with nitrogen and then contacted with a hydrogen flow of 40 cm^3/min at room temperature. The temperature was linearly raised at a rate of 2 K/min from room temperature (RT) up to 1073 K. This temperature is high enough to reduce completely the RuS_2 phase. The experiment TPR profiles evidence that during the reduction of the catalysts, H_2S is released in three temperature domains. The determination of the amount of sulfur eliminated at low, intermediate, and high temperature ranges was simply calculated by fitting the TPR profiles using commercial software working with the Marquardt–Levenberg type algorithm. The profiles were fitted without any constraints; i.e., peak position and peak shape were not imposed during the minimization process.

The solid reduction was carried out in the same experimental setup. Catalyst composition was monitored by reducing the solids at different temperatures for 2 h. Pure hydrogen was utilized for both the unsupported and silica-supported catalysts. For the zeolite-supported solid, preliminary experiments have shown that under these conditions a degree of reduction of ca. 85% was already attained at a temperature as low as 473 K. This indicates that the reduction kinetics of encaged Ru sulfide particles is very high, and hydrogen diluted in Ar (5%) was used to lower the rate of the reduction process in order to control the solid composition.

The degree of reduction (α) was defined as the ratio between the amount of H_2S eliminated upon reduction at a given temperature and the total sulfur content.

Catalytic Properties

The catalytic properties of the reduced samples have been determined at 273 K using the H_2–D_2 exchange reaction. This model reaction which involves hydrogen activation was chosen because it proceeds at a temperature lower that the one required for solid reduction. In a typical run, the catalyst was reduced at a given temperature and then cooled down to 273 K in the presence of the reducing atmosphere. The reactor was then flushed with nitrogen and the catalyst was thereafter submitted to an equimolar mixture of H_2 and D_2 diluted in Ar. The H_2 and D_2 partial pressures were 76 Torr. The variation of the H_2 and D_2 composition was analyzed by means of a mass spectrometer (FISONS Instrument) equipped with a quadrupole analyzer working in a Faraday mode. A silica capillary tube heated at 453 K continuously bled off a small fraction of the gas phase close to the reactor outlet into the spectrometer. Conversions were calculated with respect to the decrease of either the D_2 or the H_2 signals, and they were kept lower than 20% for all the solids, irrespective of their compositions, by adjustment of the contact time. It should be mentioned that under these experimental conditions, no H_2S, HDS, nor D_2S was released during the reduction course, indicating that sulfur-to-metal ratios were stable during a catalytic run.

Hydrogen Thermodesorption

The amount of hydrogen retained by the solids during the reduction treatment was first removed by thermodesorption by heating abruptly the solid from room temperature up to 573 K. Preliminary experiments had effectively shown that this temperature is high enough to desorb the hydrogen present on ruthenium sulfide based catalysts (7). Species leaving the catalyst surface were detected by a gas chromatograph equipped with a TCD detector. It was checked that during this step no H_2S was detected during these desorption experiments whatever the degree of reduction of the solids and the nature of the carrier supporting the active Ru phase. The reduced and desorbed solids were then submitted to a hydrogen flow at 273 K in order to saturate their surfaces with hydrogen, and a second thermodesorption was performed in order to quantify the amount of hydrogen retained by the solids under conditions close to those used for the determination of the catalytic activity.

Inelastic Neutron Scattering

The neutron spectra were obtained at the ISIS spallation neutron source at the Rutherford Appleton Laboratory, U.K., using the TFXA spectrometer (10). This spectrometer is a time of flight instrument with an inverse geometry and a time-focusing analyzer; it gives good counting rates and good energy transfer resolution ($\Delta E/E \sim 2\%$) over a wide range of energy transfers. The estimated precision is $\pm 10\ cm^{-1}$. For the neutron measurements, 16 g dehydrated and reduced catalyst were transferred to an aluminum container inside a glovebox.

RESULTS AND DISCUSSION

Dispersion of the Active Phase

HREM was utilized for the measurements of the average particle size of the unsupported and supported on silica ruthenium sulfide catalysts. The HREM micrographs of both samples exhibit nearly spherical particle shapes and, as shown in Fig. 1, the size distribution is rather narrow, with more than 90% of the observed spheres with a size ranging between 2.5 and 4.5 nm for the silica-supported samples and 80% for the unsupported sample. The average crystallite sizes are, respectively, 3.6 and 5 nm.

The RuS_2/KY sample was also examined by HREM. Ultrathin sections of sample grains ($\sim$20 nm) cut by ultramicrotomy were examined. A view through a cut after sulfidation shows the presence of RuS_2 particles, distributed throughout the zeolite, the mean diameter of which ranges

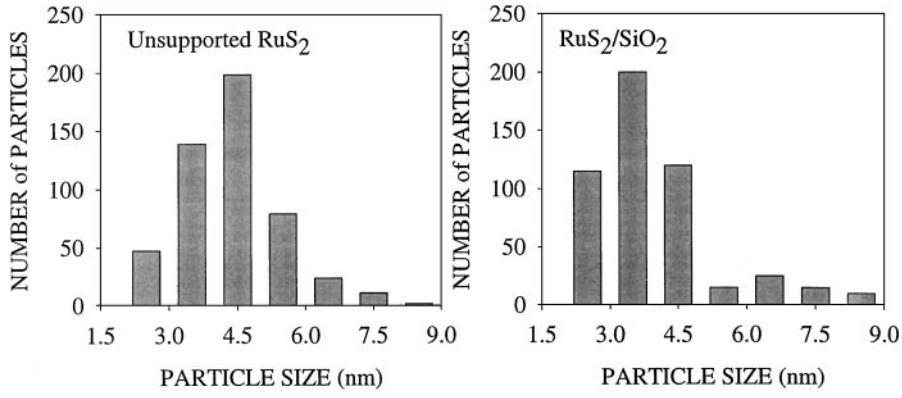

FIG. 1. Particle size distribution obtained by HREM.

from 1 to 2 nm. A few larger particles (5 to 10 nm) are located outside the lattice of the support. The obtained micrographs are very similar to those already published for ruthenium sulfide particles dispersed in a dealuminated zeolite (5). Nevertheless, it is difficult to determine accurately by HREM the size of the sulfide particles dispersed in a zeolite support. Consequently, small-angle X-ray scattering (SAXS) was also used to determine the particle diameter. The advantage of this method, compared to HREM, is that it is a volumetric method. The particle size distribution, assuming spherical particles, is shown in Fig. 2 as a function of the particle diameter. The maximum of the distribution is observed at 1.2 nm, which is close to the diameter of the supercage in the faujasite structure.

Taking into account the mean particle size determined by HREM and SAXS, the fraction of the ruthenium and sulfur ions present at the surface of the catalysts of the present study can be evaluated by the crystallographic model proposed by Geantet *et al.* (11, 12). This model is based on a three-dimensional growth of the fcc lattice of the pyrite RuS_2 structure. The structure of RuS_2 can be depicted as a modified NaCl structure with two interpenetrating fcc sublattices, one containing the Ru atoms and the other the S–S pairs. If n represents the number of unit cells at the edges of the growing polyhedra, the equations

$$Ru_t = 4n^3 + 6n^2 + 3n + 1 \quad [1]$$

$$Ru_s = 12n^2 + 2 \quad [2]$$

$$S_t = 8n^3 + 12n^2 + 6n \quad [3]$$

$$S_s = 24n^2 \quad [4]$$

are established, where S represents the number of S atoms and subscripts t and s refer, respectively, to the number of ions present on the entire particle and only at the surface. In these equations the number of unit cells n is defined by

$$n = L/\underline{a} \quad [5]$$

where L is the mean particle size as determined by HREM or SAXS and $\underline{a}$ is the lattice parameter for RuS_2 ($\underline{a}$ = 5.609 Å). Taking into account the mean particle size and the ruthenium content determined by chemical analysis, the total ruthenium content and the fraction of ruthenium present at the surface of the particles were calculated and reported in Table 2. These data show that this fraction varies in a wide domain from 0.284, for the unsupported catalyst, to

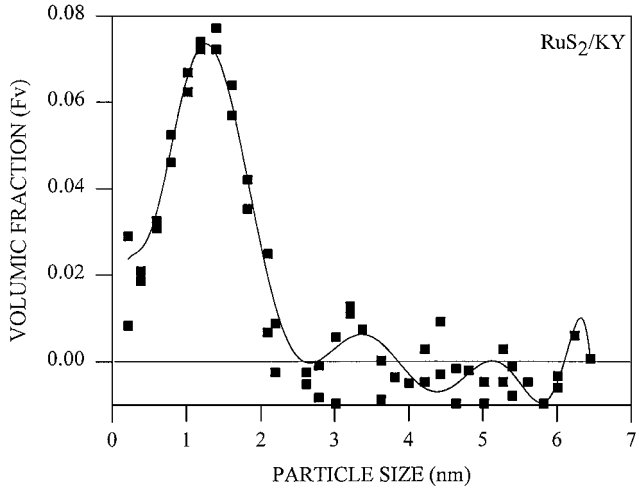

FIG. 2. SAXS determination of the particle size of RuS_2/KY.

TABLE 2

Total Ru Content Deduced from Chemical Analysis and Estimated Surface Ru Ions Calculated from the Geometrical Model Using the Cubic Model

Catalyst	Ru content (wt%)	Ru content (μmol/g)	Particle size (nm)	Ru_s/Ru_t	Ru_s (μmol/g)
$RuS_{2.27}$	58.1	5759	5	0.28(0.34)	1635(1976)
Ru/SiO_2	7.5	743	3.6	0.37(0.44)	278(328)
RuS_2/KY	8.3	822	1.2	0.77(0.79)	632(679)

Note. Data in brackets were calculated using the truncated octahedron model detailed in the text.

TABLE 3

Total S Content Deduced from Chemical Analysis and Estimated Surface and Excess S Ions Calculated from the Geometrical Model Using the Cubic Model

Catalyst	Particle size (nm)	S_t (μmol/g)	S_s (μmol/g)	S_s/S_t (μmol/g)	S_{excess}[a] (μmol/g)	S/Ru
$RuS_{2.27}$	5	11518	3291(3916)	0.28(0.34)	3681	2.6(2.9)
Ru/SiO_2	3.6	1486	555(663)	0.37(0.44)	648	2.9(3.2)
RuS_2/KY	1.2	1644	1239(1315)	0.75(0.80)	1948	4.4(5.7)

Note. Data in brackets were calculated using the truncated octahedron model detailed in the text.

[a] Calculated assuming that all Ru ions are in a sixfold sulfur coordination.

0.77, for the small particles dispersed in the zeolite. Similarly, the amount of the sulfur species can be deduced from the model. However, according to the model, the sulfur-to-metal ratio equals 2 whatever the particle size, which would mean that the ruthenium ions located at the corners and edges and those at the surface are sulfur deficient and may possess 3, 2, and 1 unsaturation, respectively. These coordinatively unsaturated sites might accommodate extra sulfur to reach the sixfold coordination state. The maximal extra sulfur anions is given by

$$S_{excess} = 24n^2 + 24n + 12. \quad [6]$$

As summarized in Table 3 the S/Ru calculated using the above model depends on the particle size and varies from 2.6, for the unsupported catalyst, to 2.9, for the silica-supported one, and may reach 4.4 for the zeolite sample. These calculated values are higher than those obtained by chemical analysis, respectively, 2.27, 2.7, and 2.5, because some sulfur vacant sites exist after the catalyst pretreatment as already discussed in Ref. 12.

This model appears likely for the biggest particles containing more than 1000 atoms, which should exhibit the monocrystal structure, while for the very small particles of RuS_2/KY, which contain less than 1000 ions, a transitional structure, i.e., octahedron, icosahedron, is more appropriate. From the cubic model described above, a truncated octahedron structure might be derived which provides a nearly spherical morphology similar to the HREM observation. The modeling of such a structure gives the equations

$$Ru_t = 16n^3 + 15n^2 + 6n + 1 \quad [7]$$

$$Ru_s = 30n^2 + 2, \quad [8]$$

the surface atoms involving 24 corner atoms, $6(n-1)^2$ atoms on square faces[100], $8(3n^2-3n+1)$ atoms on the hexagonal faces[111], $12(n-1)$ atoms on the edges between hexagonal faces, and $24(n-1)$ atoms on the edges between square and hexagonal faces. The sulfur atoms are now given by the equations

$$S_t = 32n^3 + 30n^2 + 12n \quad [9]$$

$$S_s = 60n^2 \quad [10]$$

$$S_{excess} = 60n^2 + 72n + 14. \quad [11]$$

Using these equations, the fraction of surface Ru or S ions, as well as the highest S/Ru ratio, is given in Tables 2 and 3 (data in brackets). The comparison of the two series of data shows that the fraction of surface ions does not greatly depend on the shape of the particle but mainly affects the concentration of excess sulfur atoms. However, a sixfold coordination of all the Ru ions is purely hypothetical and unrealistic in practice.

Reducibility of the Active Phase

The comportment of the three catalysts in the presence of hydrogen was studied with two different objectives. First, temperature programmed reduction was utilized to quantify the sulfur species present at the surface or in the bulk of the catalysts of the present series. Second, the reduction of the catalysts was studied under isothermal conditions in order to determine the best way (temperature, time of reduction, atmosphere) to achieve various degrees of reduction. This last study gives also valuable information on the reducibility of the active phase and consequently on its ability to form coordinatively unsaturated sites.

The TPR patterns of the three catalysts are reported in Fig. 3. These profiles show that H_2S is eliminated in three

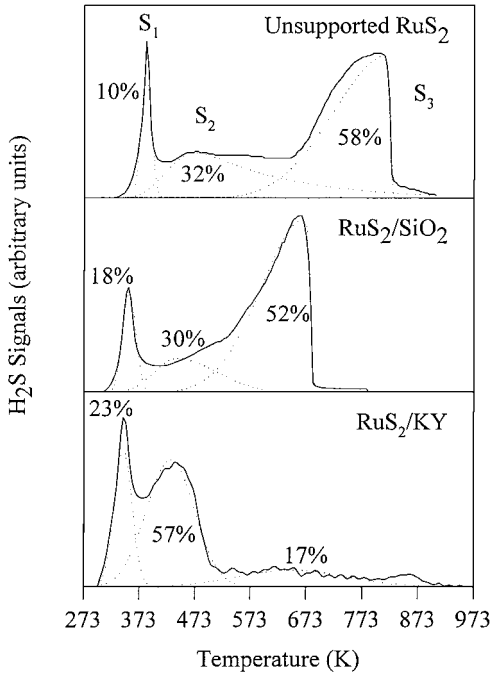

FIG. 3. TPR profiles and relative proportion of each sulfur species (denoted by S_1, S_2, and S_3 in the text).

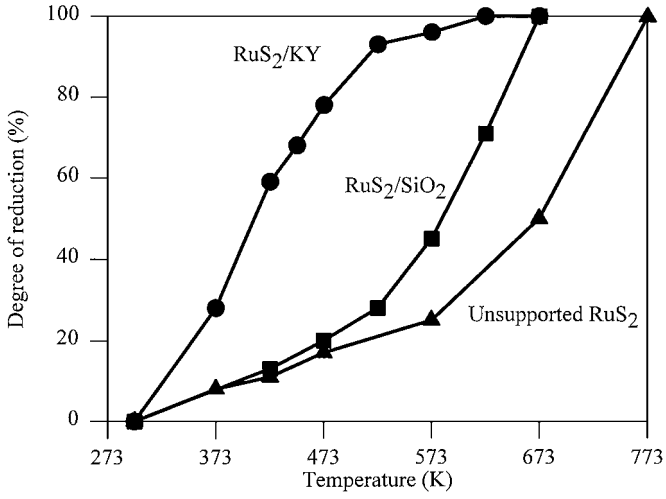

FIG. 4. Evolution of the degree of reduction versus temperature.

temperature domains. The relative amounts of S_1, S_2, and S_3 removed, respectively, at low, intermediate, and high temperature were calculated by integrating the signals, and the resulting data are also indicated in Fig. 3. Previous work has shown that the elimination of the sulfur corresponding to the low temperature peak (S_1) leads to a composition close to RuS_2, suggesting that this species could be related to the removal of the sulfur excess retained by the solid surface during the sulfiding procedure (12, 13). Assuming that the high temperature peak (S_3) corresponds to bulk sulfur elimination leading to the metallic ruthenium phase, the H_2S evolved at intermediate temperatures (S_2) has been ascribed to the removal of surface sulfur anion. As expected, due to the different particle sizes of the catalysts, the relative areas of peaks 2 and 3 vary in a wide range from the unsupported catalysts to the small clusters dispersed in the zeolite

TABLE 4

Experimental and Calculated Fractions of Surface S Anions

Catalyst	$S_2(S_2+S_3)$ (from TPR)	S_s/S_t (cubic model)	S_s/S_t (truncated octahedron model)
RuS_2	0.35	0.28	0.34
RuS_2/SiO_2	0.37	0.37	0.44
RuS_2/KY	0.77	0.75	0.80

(Table 4). The experimental $S_2/(S_2+S_3)$ data are within the experimental errors in fairly good agreement with the calculated S_s/S_t, independent of the model used. These data strongly support the proposed sulfur species assignment.

Figure 4 shows the variation of the degree of reduction of the three solids investigated as a function of the temperature. Results clearly evidence the influence of particle size on solid reducibility, which is higher for the silica-supported sample than for the unsupported one. This effect is even more pronounced for the zeolite catalyst despite of the use of diluted hydrogen. In this set of experiments, hydrogen was left flowing for 2 h until no H_2S was released. This allows a precise monitoring of the composition of the catalysts.

Catalytic Properties

The catalytic properties of the catalysts of the present series as a function of α are illustrated in Fig. 5. Preliminary experiments have shown that both supports are not active in this reaction. The activity increases upon sulfur removal and reaches a maximum whose position depends on the particle size of the sulfided phase. For instance, the α values leading to the maximum activities are 0.38 and 0.55 for the unsupported and silica-supported catalysts which

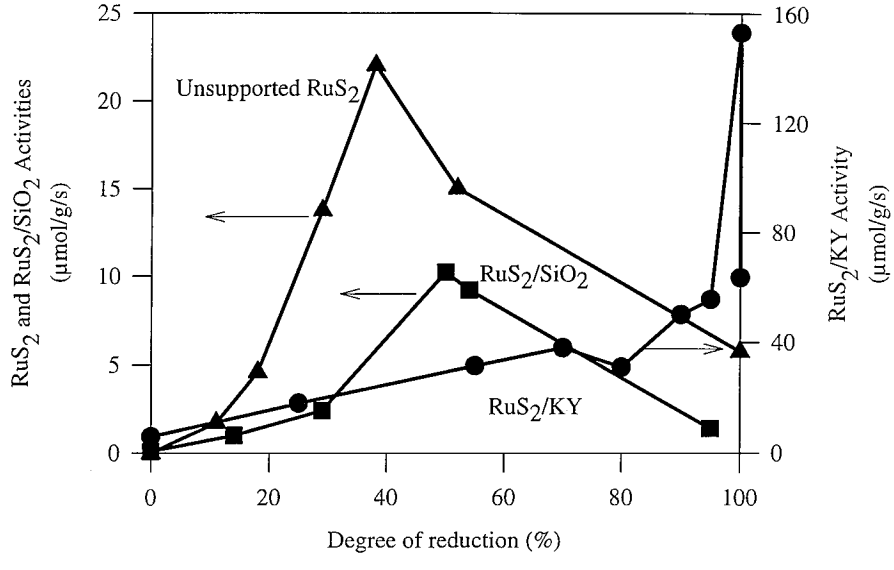

FIG. 5. H_2–D_2 exchange activities as a function of the degree of reduction.

are close to the elimination of the excess and superficial sulfur atoms, i.e., 42 and 48%, respectively (see Fig. 3). For higher reduction states, the activity decrease was previously ascribed to solid sintering and to the replacement of the active sulfide phase by a poisoned metallic phase (7). For the zeolite-supported system the activity first increases up to ~0.7 and then declines before exhibiting a drastic enhancement when α approaches 1. The first maximum could be also related to surface sulfur depletion while for further reduction the high increase of activity may be interpreted in terms of formation of small metallic particles. For the latter, the formation of a less poisoned metallic phase might be ascribed to both the high dispersion and the zeolitic environment (14).

Hydrogen Thermodesorption

The hydrogen thermodesorption profiles recorded for various degrees of reduction (α) of the silica-supported sample are reported in Fig. 6. The shape of the resulting spectra differs depending on the solid composition. For instance, at low reduction stage ($\alpha = 0.14$) a large peak centered around 485 K is observed. The intensity of this peak declines for $\alpha = 0.28$, and a second desorption peak is detected at 430 K and only the latter is present for highly sulfur-depleted surfaces. This comportment is extremely similar to the one observed and already reported for the unsupported ruthenium sulfide catalyst (7, 15). These TPD profiles evidence the presence of at least two types of hydrogen species adsorbed on the surface of reduced ruthenium sulfide, either unsupported or supported on silica, the relative concentration of which depends on the degree of reduction of the sample as shown in Fig. 7. The concentration of the species desorbing at high temperature (HT) is already high for low values of α and becomes almost undetectable when the surface is poorly covered by sulfur. By contrast, the concentration of the species desorbing at low temperature (LT) reaches a maximum for these reduced states ($\alpha = 0.35$ and 0.5) and follows the same trend as the activity does. For the unsupported sample, the nature of these adsorbed species has been elucidated by ^{1}H NMR and INS (3, 16). These techniques have evidenced that the LT species may be related to the homolytic adsorption of dihydrogen on Ru centers in a low sulfur coordination while the HT species reflect an heterolytic dissociation on an Ru–S site leading to Ru–H and SH groups. The comparison of these adsorption results with those obtained for the H_2–D_2 exchange reaction evidences a striking similarity in the variations with α of the activity and the $[H_2]_{LT}$.

For RuS_2/KY the TPD profile (Fig. 8) does not change so drastically with α. Two species are observed even for a high degree of reduction, and their relative concentration is

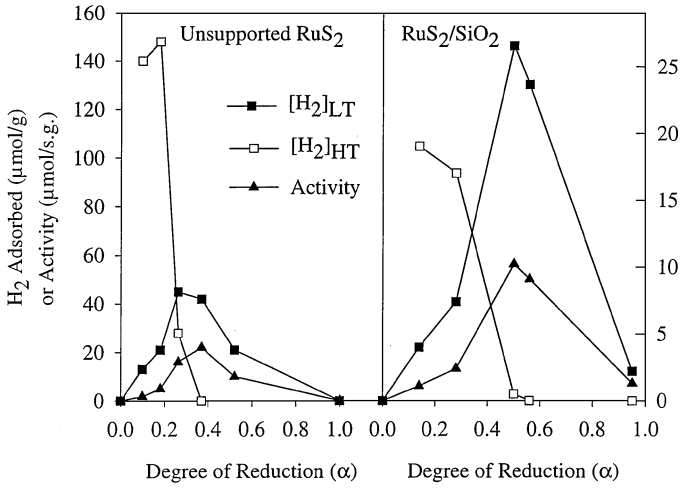

FIG. 7. Evolution of the exchange activity and of the concentration of the low and high temperature hydrogen desorption peak versus the degree of reduction for unsupported and silica-supported RuS_2.

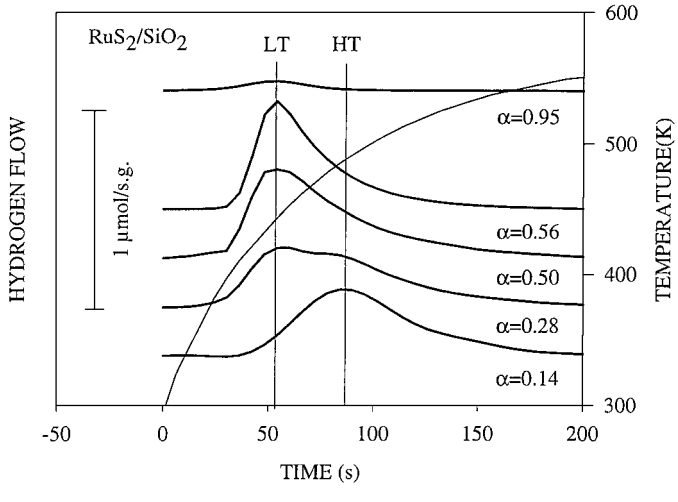

FIG. 6. Hydrogen TPD profile observed for RuS_2/SiO_2 for various reduction states (α).

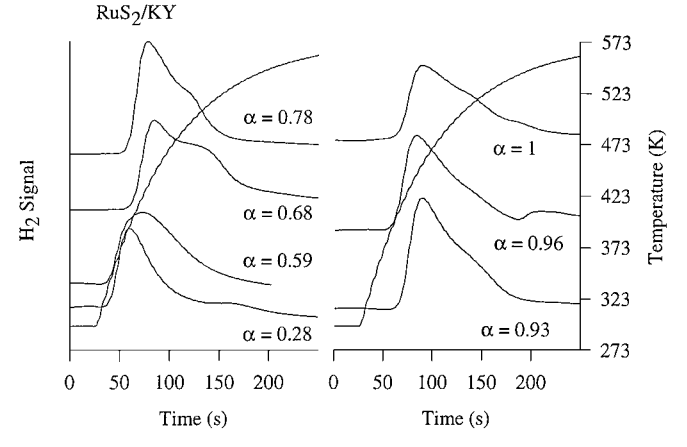

FIG. 8. Hydrogen TPD profile observed for RuS_2/KY for various reduction states (α).

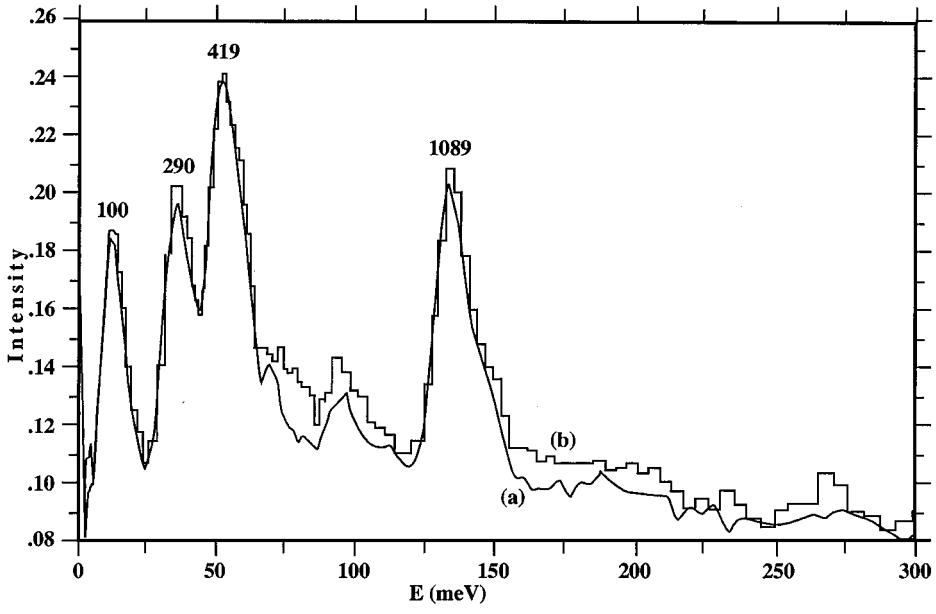

FIG. 9. INS spectra of (a) degassed RuS_2/KY and (b) hydrogen adsorbed at 25 K (the values within the figure are the transition frequencies in cm^{-1}).

not really modified. In order to elucidate the origin of this difference, in comparison to the other samples, the nature of the adsorbed hydrogen species was studied by INS.

Inelastic Neutron Scattering

A background run was performed with the bare catalyst, RuS_2/KY, placed in a cryostat at 25 K; the resulting spectrum is shown in Fig. 9 (curve a). The intense peaks measured at 419 and 1089 cm^{-1} are due, respectively, to the out-of-plane and the in-plane bending modes of bridged hydroxyl groups (16–18) while the bands at 100 and 290 cm^{-1} correspond to phonons of the aluminum container.

Hydrogen adsorption was performed at room temperature after the cell was taken out of the cryostat. A pressure of 700 mbar was applied onto the catalyst and the sample was left 12 h to equilibrate. After this, gaseous hydrogen was removed and the final pressure in the cell was ~1 mbar. The sample was cooled down to 25 K and a new INS spectrum was obtained and is given in Fig. 9 (curve b). Such a low temperature is used to sharpen the local modes of hydrogen by reducing the effect of the Debye–Waller factor (19). It is clear that the modification of the signal after hydrogen adsorption is rather weak, which is reflected by the large error bars in the difference spectrum in Fig. 10.

Even if the quantity of hydrogen adsorbed on the supported RuS_2 particles is relatively small for a neutron experiment, several INS peaks can nevertheless be observed in the difference spectrum, Fig. 10. A comparison is made in the same figure with the spectrum already reported for hydrogen adsorbed on unsupported RuS_2 (3). The spectral region 320–1300 cm^{-1} was previously found to contain all the fundamental modes of the different hydrogen species. The vibrational peaks at 645 and 720 cm^{-1} in Fig. 10 were assigned to SH bending modes and those at 542 and 826 cm^{-1} to the bending modes of two different RuH linear species. Similar bands are found for supported RuS_2: the bands at 637, 673, and 710 cm^{-1} can be assigned to SH groups and those at 541 and 823 cm^{-1} to RuH species. In previous INS studies performed on sulfides, SH bending modes were reported at 650 cm^{-1} on MoS_2 (20), at 694 cm^{-1} on WS_2 (21), and at 600 and 710 cm^{-1} on RuS_2 (22). The peak at 593 cm^{-1} might then be assigned either to an SH or to a RuH bend, but the band at 757 cm^{-1} is definitely out of the range of the SH bends and is thus assigned to another RuH species. From this technique, it appears that in addition to heterolytic adsorption RuH species must arise also from homolytic adsorption on different ruthenium sites. According to the low particle size, it is effectively expected that the cluster may offer different crystallographic orientations. Thus this vibrational technique allows the detection of various species which cannot be resolved by TPD.

Hydrogen Adsorption and Catalytic Activities

For unsupported RuS_2 catalyst, Fig. 11 shows that the activity is directly proportional to the amount of LT species. Interestingly, the data corresponding to the silica-supported catalyst are aligned on the same straight line. This means that the activity per site able to form RuH species is similar for both catalysts. For the zeolite system, the relation of the catalytic activity with the LT peak is also linear but the slope is only twice as high as the one determined for the two other solids. Theoretical ab initio calculations have been

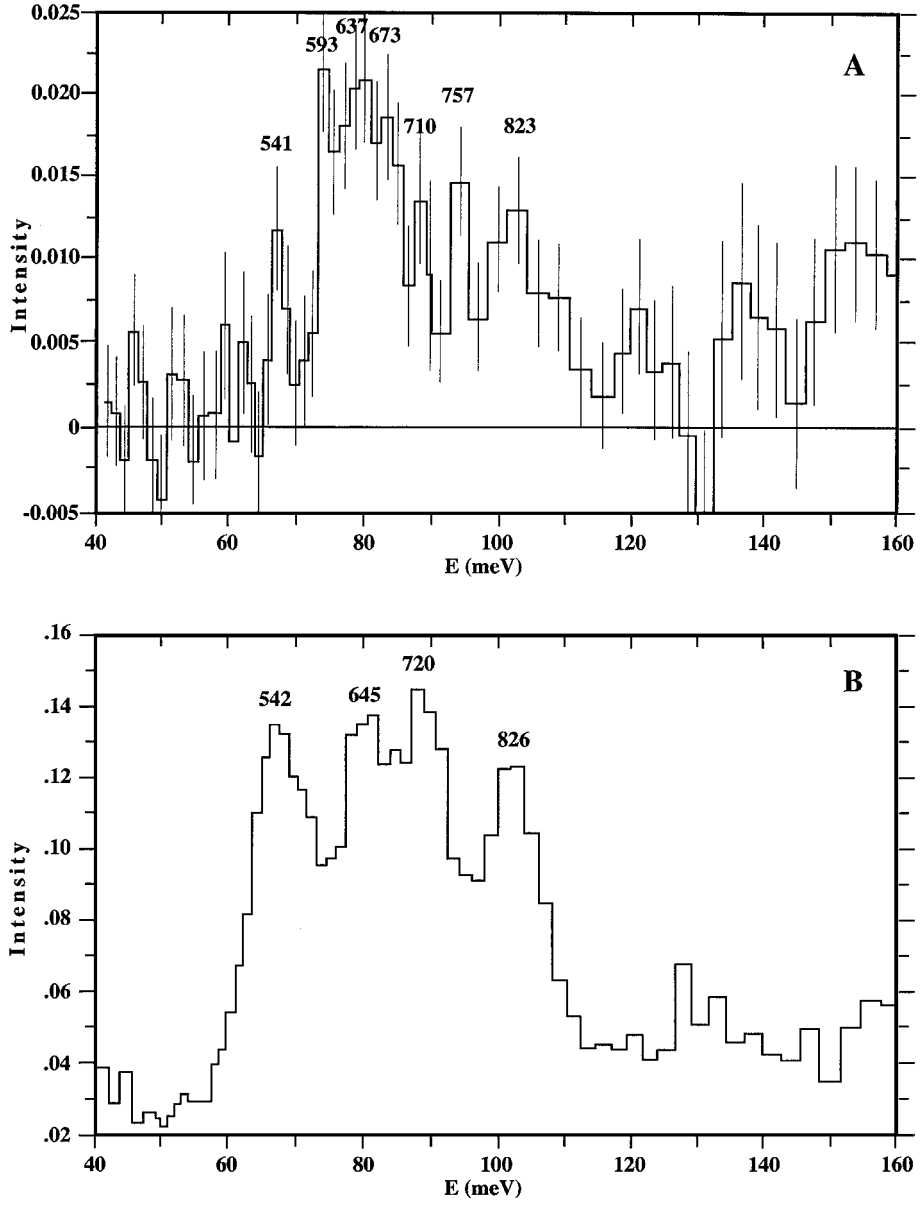

FIG. 10. (A) INS spectrum of hydrogen adsorbed on RuS_2/KY (the signal of the bare catalyst has been substracted and the error bars schematized). (B) INS spectrum of hydrogen adsorbed on unsupported RuS_2.

recently performed on the interaction of hydrogen with [100] and [111] RuS_2 surfaces (23–24). These authors have concluded that the [111] face is more reactive than the [100] one. Taking into account this result, the higher turnover frequency observed on the RuS_2/KY might arise from a higher density of [111] planes related to the very small size of the sulfided cluster.

CONCLUSIONS

This work has evidenced the possibility of preparing RuS_2-based catalyst in a wide range of particle sizes. Indeed, the use of a zeolite-type support allows us to stabilize very small clusters of the RuS_2 pyrite phase. The observed particle size is roughly three to four times lower than those obtained on conventional supports such as silica or alumina (4). The TPR patterns consist of three domains of H_2S removal whatever the particle size. As every TPR peak represents a distinct reduction process involving a particular component of the solid, this shows that the support does not greatly affect the reduction steps of the active phase. Coupling these results with solid modeling, each peak has been ascribed to the elimination of excess sulfur atoms, surface sulfur, and bulk. The area underneath each component allows the determination of the amount of each sulfur species. The particle size greatly influences the relative amount of

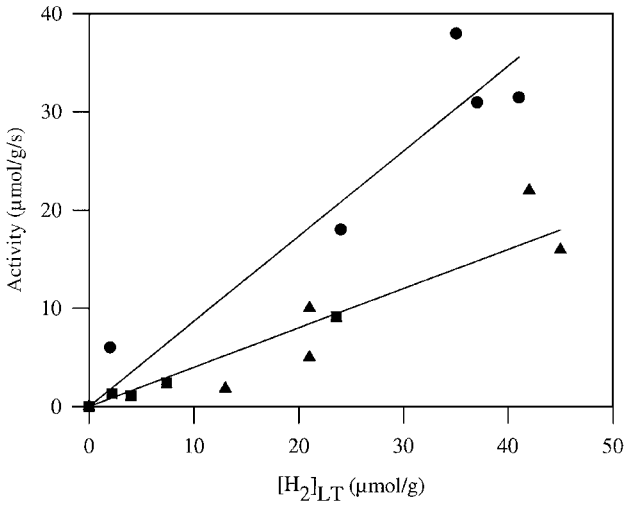

FIG. 11. Linear relationship between the catalytic activity and the low temperature hydrogen species: ▲, RuS_2; ■, RuS_2/SiO_2; ●, RuS_2/KY.

each sulfur species and the experimental data are in excellent agreement with the predicted ones. Besides this aspect, it was observed that the dispersion favors the RuS_2 reducibility by decreasing the position of peak maxima.

For unsupported RuS_2, it was reported that hydrogen adsorption depends on the S/Ru ratio and two different species were characterized using either INS or ^1H NMR (3, 15). At high S/Ru ratio hydrogen may dissociate heterolitically on a coordinatively unsaturated Ru site and a sulfur anion giving rise to Ru–H and SH moieties. As far as sulfur is removed upon reduction an homolytic mechanism occurs on low coordinated Ru sites. A similar behavior is observed on the silica-supported sample. For the zeolite supported material, the INS characterization has revealed the presence of some SH groups and various Ru–H species. This suggests the existence of several low coordinated Ru sites as might be expected due to the very small cluster size.

The determination of the H_2–D_2 activity has evidenced that a fully sulfur-saturated catalyst is not active for hydrogen activation whatever the dispersion of the RuS_2 phase. The activity increases with solid reduction, and a maximum appears for an almost sulfur-depleted surface. After this maximum, the decrease of catalytic activity is due to the fomation of bulky metallic ruthenium phases poisoned by sulfur. Up to the S/Ru ratio corresponding to the maximum of activity, the determination of turnover numbers gives similar results for unsupported or supported on silica ruthenium sulfide. For the zeolite sample, the turnover number is at most two times higher than for the above samples which might be ascribed to a larger amount of the most reactive [111] planes. It seems that the interest of using this zeolite is the stabilization of nanoparticles of a sulfide phase which cannot be realized on an oxide surface such as silica or alumina. However, a superimposed effect of the zeolite environment on the properties of a sulfide phase might be observed for acidic zeolites. This influence is very large and can reach a factor of 200 as reported recently for the hydrogenation of tetraline carried out on a series of Y zeolites with various acidic properties (6). The present work represents the base study which would allow us to distinguish what in the general term support interaction is related to the size of the particle or what is due to the modification of the site property of the support and the active phase.

REFERENCES

1. Pecoraro, T. A., and Chianelli, R. R., *J. Catal.* **67**, 430 (1981).
2. Lacroix, M., Boutarfa, N., Guillard, C., Vrinat, M., and Breysse, M., *J. Catal.* **120**, 473 (1989).
3. Jobic, H., Clugnet, G., Lacroix, M., Yuan, S., Mirodatos, C., and Breysse, M., *J. Am. Chem. Soc.* **115**, 3654 (1993).
4. Geantet, C., Göbölös, S., De los Reyes, J. A., Cattenot, M., Vrinat, M., and Breysse, M., *Catal. Today* **10**, 665 (1991).
5. Moraweck, B., Bergeret, G., Cattenot, M., Kougionas, V., Geantet, C., Portefaix, J. L., and Breysse, M., *J. Catal.* **165**, 45 (1997).
6. Breysse, M., Cattenot, M., Kougionas, V., Lavalley, J. C., Mauge, F., Portefaix, J. L., and Zotin, J. L., *J. Catal.* **168**, 143 (1997).
7. Lacroix, M., Mirodatos, C., Breysse, M., Décamp, T., and Yuan, S., *in* "New Frontiers in Catalysis" (L. Guczi, F. Solymosi, and P. Tétényi, Eds.), p. 597. Elsevier, Budapest, 1993.
8. Knop, O., *Can. J. Chem.* **41**, 1838 (1963).
9. Renouprez, A., Bottazi, H., Weigel, D., and Imelik, B., *J. Chem. Phys.* **62**, 131 (1965).
10. Penfold, J., and Tomkinson, J., Rutherford Appleton Laboratory Report, RAL-86-019, 1986.
11. Geantet, C., Calais, C., and Lacroix, M., *Compt. Rend. Acad. Sci. Paris* **315 Série II**, 339 (1992).
12. Berhault, G., Lacroix, M., Breysse, M., Maugé, F., Lavalley, J.-C., and Qu, L. L., *J. Catal.* **170**, 37 (1997).
13. Labruyère, F., Lacroix, M., Schweich, D., and Breysse, M., *J. Catal.* **167**, 464 (1997).
14. Bartholomew, C. H., Agrawal, P. K., and Katzer, J. R., *Adv. Catal.* **31**, 135 (1982).
15. Lacroix, M., Yuan, S., Breysse, M., Dorémieux-Morin, C., and Fraissard, J., *J. Catal.* **138**, 409 (1992).
16. Jobic, H., *J. Catal.* **131**, 289 (1991).
17. Jacobs, W. P. J. H., Jobic, H., van Wolput, J. H. M. C., and van Santen, R. A., *Zeolites* **12**, 315 (1992).
18. Jacobs, W. P. J. H., van Wolput, J. H. M. C., van Santen, R. A., and Jobic, H., *Zeolites* **14**, 117 (1994).
19. Jobic, H., and Lauter, H. J., *J. Chem. Phys.* **88**, 5450 (1988).
20. Sampson, C., Thomas, J. M., Vasudevan, S., and Wright, C. J., *Bull. Soc. Chim. Belg.* **90**, 1215 (1981).
21. Wright, C. J., Fraser, D., Moyes, R. B., and Wells, P. B., *Appl. Catal.* **1**, 49 (1981).
22. Heise, W. H., Lu, K., Kuo, Y. J., Udovic, T. J., Rush, J. J., and Tatarchuk, B. J., *J. Phys. Chem.* **92**, 5184 (1988).
23. Frechard, F., and Sautet, P., *Surf. Sci.* **389**, 31 (1997).
24. Frechard, F., and Sautet, P., *J. Catal.* **170**, 402 (1997).